Supplementary Information:

Reversible change of luster color from pale yellow to wine red in microcrystalline film by photochromic diarylethene having a naphthyl group

Ryotaro Shiromae,[a] Yuma Nakagawa,[a,b] Shota Watanabe,[a] Ryo Nishimura,[c] Masakazu Morimoto,[c] Satoshi Yokojima,[d] Shinichiro Nakamura,[e] Kingo Uchida[a*]*

[a] Department of Materials Chemistry, Faculty of Science and Technology, Ryukoku University, Seta, Otsu, Shiga 520-2194, Japan.

[b] Molecular Engineering Institute, Shiga University of Medical Science, Seta, Otsu, Shiga 520-2192, Japan.

[c] Department of Chemistry and Research Center for Smart Molecules, Rikkyo University, 3-34-1 Nishi-Ikebukuro, Toshima-ku, Tokyo 171-8501, Japan.

[d] School of Pharmacy, Tokyo University of Pharmacy and Life Sciences, 1432-1 Horinouchi, Hachioji, Tokyo 192-0392, Japan.

[e] Priority Organization by Innovation and Excellence, Laboratory for Data Science, Kumamoto University, 2-39-1 Kurokami, Chuo-ku, Kumamoto 860-8555, Japan.

**E-mail: nyuma@belle.shiga-med.ac.jp (Y.N.)*

uchida@rins.ryukoku.ac.jp (K.U.)

----------Table of Contents----------

Materials and Methods

1. Materials

All commercial reagents were used as received unless otherwise stated.

2. General information

^{1}H (400 MHz) spectra were recorded with a JEOL JNM-400 spectrometer. Chemical shifts are reported in ppm from the signals of tetramethylsilane (TMS) for ^{1}H NMR (TMS: 0.00 ppm, s),[S1] solvent peak for ^{13}C NMR ($CHCl_3$: 77.16 ppm),[S1] and hexafluorobenzene (C_6F_6) for ^{19}F NMR (C_6F_6: -164.9 ppm) in $CDCl_3$. . In the case of molecules with perfluorocyclopentene rings, the ^{13}C NMR measurement by the ^{1}H decoupling method lacks signals from the fluorine-bondedcarbon atoms. To measure these missing signals, we performed ^{13}C NMR measurements using the ^{19}F decoupling method. However, the ^{13}C NMR using the ^{19}F decoupling method gave no clear data because the peaks were split by ^{1}H coupling. Note, therefore, that the ^{13}C NMR data in this paper were measured using the standard ^{1}H decoupling method. The absorption and reflection spectra were measured with a Hitachi U-4150 spectrophotometer. Specular reflection spectra were measured with a Shimadzu UV-3100 spectrophotometer with an attached 5-degree relative specular reflectance accessory. XRD spectra were measured with a Rigaku RINT2500 (CuKα: 1.5418 Å). SEM images were recorded using a KEYENCE VE-8800. For UV light irradiation, a UV hand lamp SPECTROLINE Model EB-280C/J (λ = 313 nm) and an As ONE Handy UV Lamp LUV-6 (λ = 365 nm, 810 μW cm^{-2}) were used. For visible light irradiation, a HAYASHI-REPIC LUMINAR ACE Model LA-HDF108AA, attached with NPI PLG-1-500V-6, PCL21, and PYF-22.5 (λ > 480 nm), was used. Crystal sizes were calculated from photographs taken using ImageJ software.[S2] All measurements and observations were performed at room temperature unless otherwise specified.

3. Single-crystal X-ray diffraction (SC-XRD) analysis

The SC-XRD analysis for the crystal of **1o** irradiated with λ = 365 nm light (ASASHI SPEXTRA CL-1501 attached with CL-H1-365-9-1 and CL-H1LCB01) was performed with an X-ray diffractometer (Bruker AXS, D8 QUEST) and MoKα radiation (λ = 0.71073 Å). The crystal was cooled using a low-temperature controller (Japan Thermal Engineering, JAN 2-12). The diffraction by frames was integrated with the Bruker SAINT program. The cell constants were determined by global refinement. The data were corrected for absorption effects using the multi-scan method (SADABS). The structure

was solved by the direct method and refined by the full-matrix least-squares method using the SHELX2014 program. The positions of all hydrogen atoms were calculated geometrically and refined by the riding model. The crystallographic data can be obtained free of charge from the Cambridge Crystallographic Data Centre via www.ccdc.cam.ac.uk/data_request/cif (CCDC No. 2313640 and 2313753).

4. Calculation of color coordinates for optical color change characteristics

To calculate the CIELAB color coordinates[S3] of **1o-film** before and after light irradiation, the L^* (lightness), a^* (red-green), and b^* (yellow-blue) values of the measured reflection spectrum were calculated using the Hitachi color calculation program. The color change values were calculated from the photometric values in the wavelength range (380–780 nm) as tristimulus values (X, Y, Z) using the following equations:

$$X = \frac{\int_{380}^{780} S(\lambda) \cdot R(\lambda) \cdot x(\lambda) d\lambda}{\int_{380}^{780} S(\lambda) \cdot y(\lambda) d\lambda}, \qquad (1)$$

$$Y = \frac{\int_{380}^{780} S(\lambda) \cdot R(\lambda) \cdot y(\lambda) d\lambda}{\int_{380}^{780} S(\lambda) \cdot y(\lambda) d\lambda}, \qquad (2)$$

$$Z = \frac{\int_{380}^{780} S(\lambda) \cdot R(\lambda) \cdot z(\lambda) d\lambda}{\int_{380}^{780} S(\lambda) \cdot y(\lambda) d\lambda}, \qquad (3)$$

where $S(\lambda)$ is the spectral distribution of the standard illuminant as defined by the International Commission on Illumination (D65)[S4], $R(\lambda)$ is the spectral reflectance, and $x(\lambda)$, $y(\lambda)$, and $z(\lambda)$ are isochromatic functions in a 10° field of view[S5]. Using these obtained values, the lightness (L^*) and color coordinates (a^*, b^*) were calculated from the equations below:

$$L^* = 116\left(\frac{Y}{Y_n}\right)^{\frac{1}{3}} - 16, \qquad (4)$$

$$a^* = 500\left[\left(\frac{X}{X_n}\right)^{\frac{1}{3}} - \left(\frac{Y}{Y_n}\right)^{\frac{1}{3}}\right], \qquad (5)$$

$$b^* = 200\left[\left(\frac{Y}{Y_n}\right)^{\frac{1}{3}} - \left(\frac{Z}{Z_n}\right)^{\frac{1}{3}}\right], \qquad (6)$$

where X_n, Y_n, and Z_n are the tristimulus values (X_n = 94.810, Y_n = 100, Z_n =107.322) for a

perfectly diffuse reflective surface with a 10° field of view under D65 illumination.

5. Synthesis of 1

The synthetic route of **1o** is shown in scheme S1.

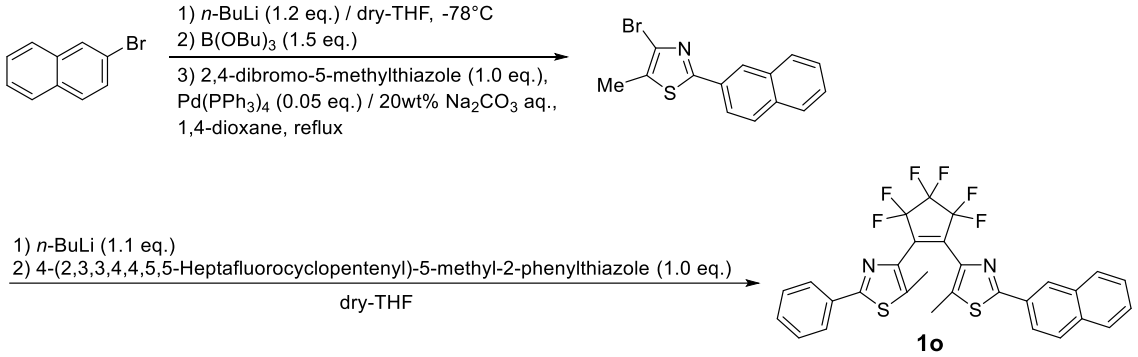

Scheme S1. Synthetic route of 1-(5-methyl-2-phenylthiazole-4-yl)-2-(5-methyl-2-naphthylthiazole-4-yl)perfluorocyclopentene (**1o**).

4-Bromo-5-methyl-2-(2-naphthyl)thiazole

Into a 300-mL three-neck flask, 4.86 g (23.4 mmol) of 2-bromonaphthalene was added to 100 mL of THF anhydrous in a dry ice-methanol bath at -78°C in an argon gas atmosphere. To the solution, 17.5 mL (28.0 mmol, 1.2 eq.) of 1.6 N *n*-BuLi in an *n*-hexane solution was gradually added while maintaining the temperature and stirred for 1 h at this temperature. Then 8.1 mL (30.3 mmol, 1.3 eq.) of tributyl borate was added, followed by stirring another 30 min, after which the temperature of the reaction mixture was allowed to warm to room temperature. Then the mixture was stirred for 1 h at this temperature. After the reaction was complete, the solvents were evaporated in vacuo. To the reaction mixture, we added 2,4-dibromo-5-methylthiazole[S6] (6.00 g, 23.4 mmol, 1.0 eq.), tetrakis(triphenylphosphine)palladium(0) (1.35 g, 1.17 mmol, 0.05 eq.), 20 wt% Na_2CO_3 aq. (60 mL), and 1,4-dioxane (120 mL), and then the mixture was refluxed for 18 h. After the reaction was complete, the reaction mixture was allowed to cool to room temperature, followed by the addition of water (300 mL). The mixture was extracted with 50 mL of diethyl ether five times. The organic layer was dried over sodium sulfate anhydrous. After removal of sodium sulfate by filtration, the solvents were removed in vacuo. The resulting crude product was purified by column chromatography on silica gel using a mixture of *n*-hexane and ethyl acetate (98:2 (v/v)) as an eluent to obtain 6.30 g of crude product. By

recrystallization from *n*-hexane, 4.72 g (15.5 mmol) of the 4-bromo-5-methyl-2-(2-naphthyl)thiazole was obtained as colorless needle crystals in 70% yield.

m.p. 108.0−108.6°C. ^{1}H NMR (400 MHz, $CDCl_3$, ppm: Figure S1) δ 8.37 (s, 1 H), 7.97 (dd, J = 8.8, 1.6 Hz, 1H), 7.92-7.84 (m, 3H), 7.52 (ddd, 9.6, 3.6, 3.2 Hz, 2H), 2.48 (s, 3H). ^{13}C NMR (100 MHz, $CDCl_3$, ppm: Figure S2) δ 165.6, 134.3, 133.3, 130.3, 129.0, 128.9, 128.8, 128.0, 127.3, 127.0, 125.6, 125.5, 123.5, 13.2. Anal. Calcd for $C_{14}H_{10}BrNS$: C, 55.28; H, 3.31; N, 4.60. Found: C, 55.39; H, 3.27; N, 4.42.

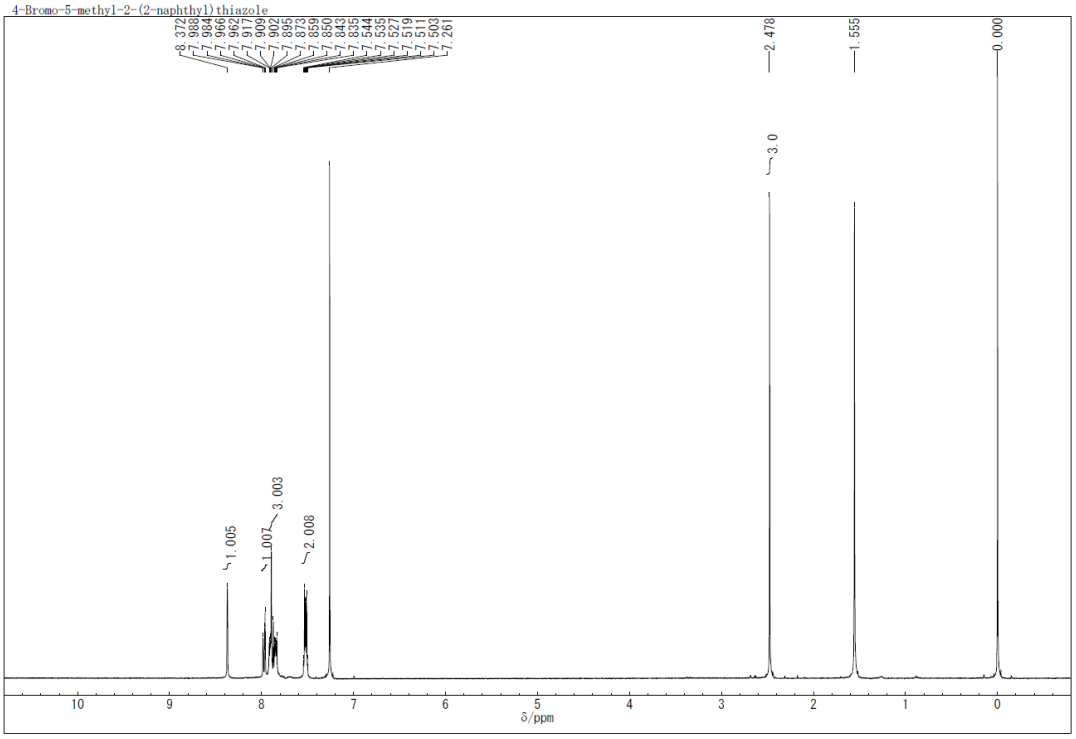

Figure S1. ^{1}H NMR ($CDCl_3$, 400 MHz) spectrum of 4-bromo-5-methyl-2-(2-naphthyl)thiazole.

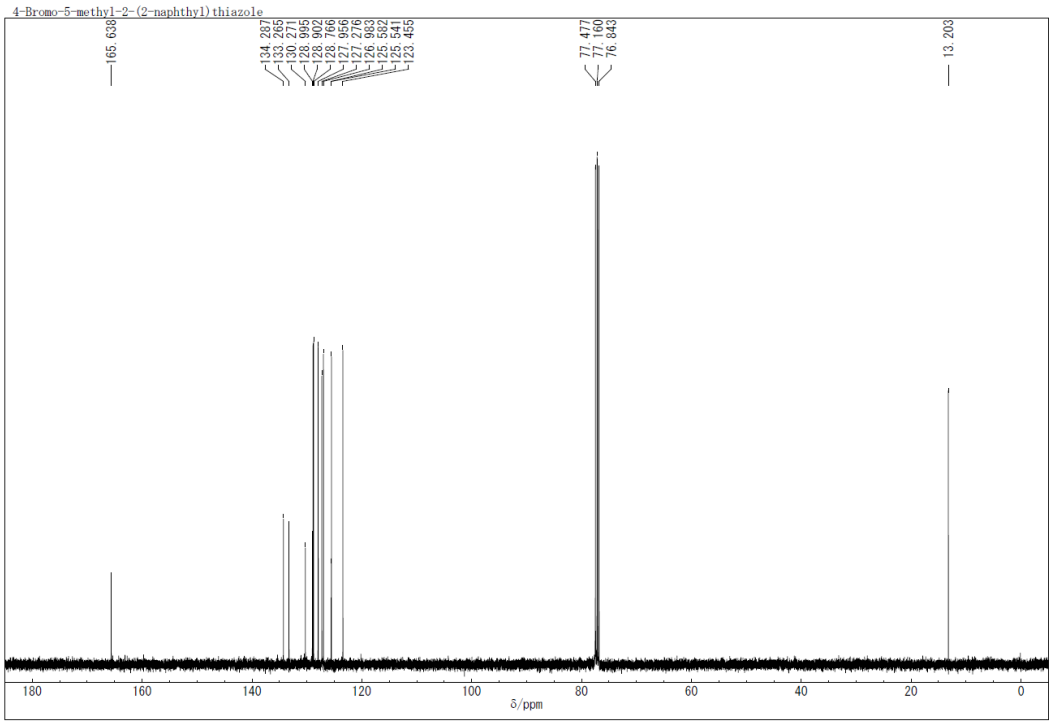

Figure S2. ^{13}C NMR ($CDCl_3$, 100 MHz) spectrum of 4-bromo-5-methyl-2-(2-naphthyl)thiazole.

1-(5-Methyl-2-phenylthiazol-4-yl)-2-[5-methyl-2-(2-naphthyl)thiazol-4-yl]perfluorocyclopentene (1o)

Into a 100-mL three–neck flask, 1.42 g (4.90 mmol) of 4-bromo-5-methyl-2-(2-naphthyl)thiazole was added to 20 mL of THF anhydrous in a dry ice-methanol bath at -78°C in an argon gas atmosphere. To this solution, 3.7 mL (5.9 mmol, 1.2 eq.) of 1.6 N *n*-BuLi in *n*-hexane solution was gradually added while maintaining the temperature and stirred for 1 h at this temperature. To the mixture, THF anhydrous solution containing 1.80 g (4.90 mmol, 1.0 eq.) of 4-(2,3,3,4,4,5,5-heptafluorocyclopentenyl)-5-methyl-2-phenylthiazole[S7] was added, followed by stirring for another 10 min. The temperature of the reaction mixture was allowed to warm to -40°C, and then the solution was stirred another 4 h at this temperature. After the reaction was completed, 10 mL of water was added, and the mixture was allowed to warm to room temperature. The solvents were evaporated in vacuo, then 200 mL of water was added. The mixture was extracted with 50 mL of diethyl ether five times. The organic layer was dried over sodium sulfate anhydrous. After removal of sodium sulfate by filtration, the solvents were removed in vacuo. The resulting crude product was purified by column chromatography on silica gel using a mixture of hexane and dichloromethane (3:1 (v/v)) as an eluent to obtain 1.29 g

(2.25 mmol) of **1o** as pale yellow solid in 46% yield.

m.p. 117.2−118.2°C. ^{1}H NMR (400 MHz, $CDCl_3$, ppm: Figure S3) δ 8.32 (s, 1 H), 7.98 (dd, J = 8.8, 1.6 Hz, 1H), 7.90-7.84 (m, 5H), 7.55-7.49 (m, 2H), 7.44-7.41 (m, 3H), 2.15 (s, 3H), 2.13 (s, 3H). ^{13}C NMR (100 MHz, $CDCl_3$, ppm: Figure S4) δ 166.0, 165.9, 140.6, 140.5, 137.4, 137.2, 134.4, 133.3, 133.1, 130.5, 130.5, 129.1, 128.9, 128.8, 128.0, 127.3, 127.0, 126.6, 126.2, 123.9, 12.4, 12.3. 19F NMR (376 MHz, $CDCl_3$, ppm: Figure S5) δ -113.6 (s, 2 F), -113.7 (s, 2F), -135.2 (s, 2F). Anal. Calcd for $C_{29}H_{18}F_6N_2S_2$: C, 60.83; H, 3.17; N, 4.89. Found: C, 60.55; H, 3.04; N, 4.83.

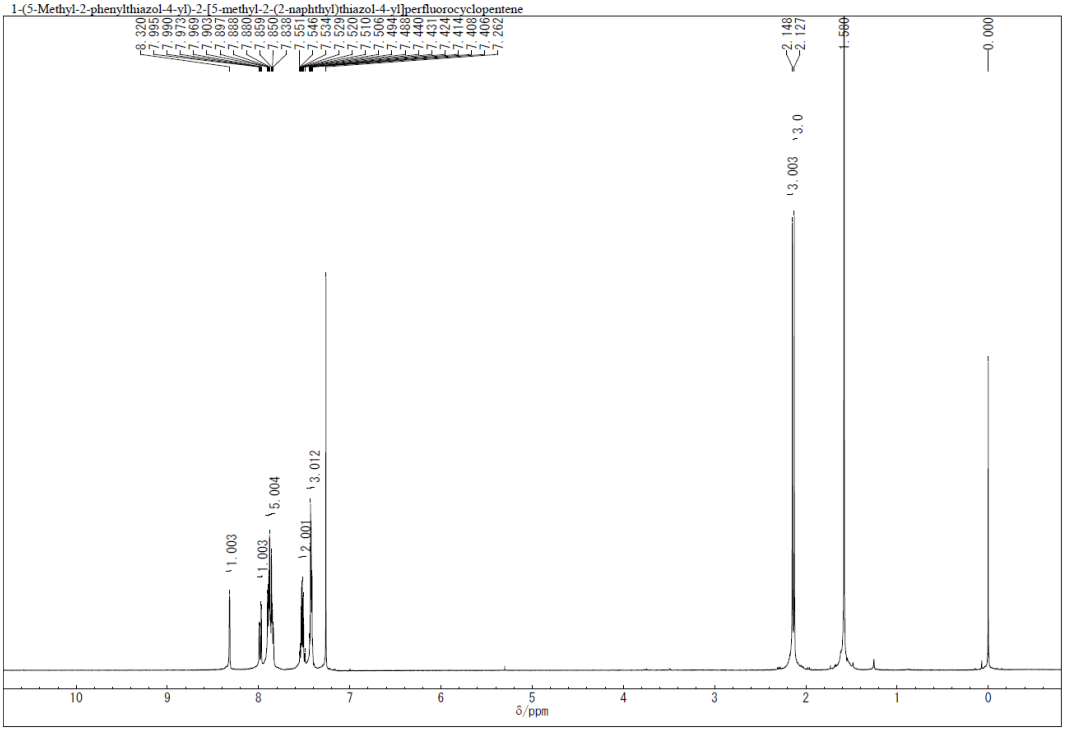

Figure S3. ^{1}H NMR ($CDCl_3$, 400 MHz) spectrum of 1-(5-methyl-2-phenylthiazol-4-yl)-2-[5-methyl-2-(2-naphthyl)thiazol-4-yl]perfluorocyclopentene (**1o**).

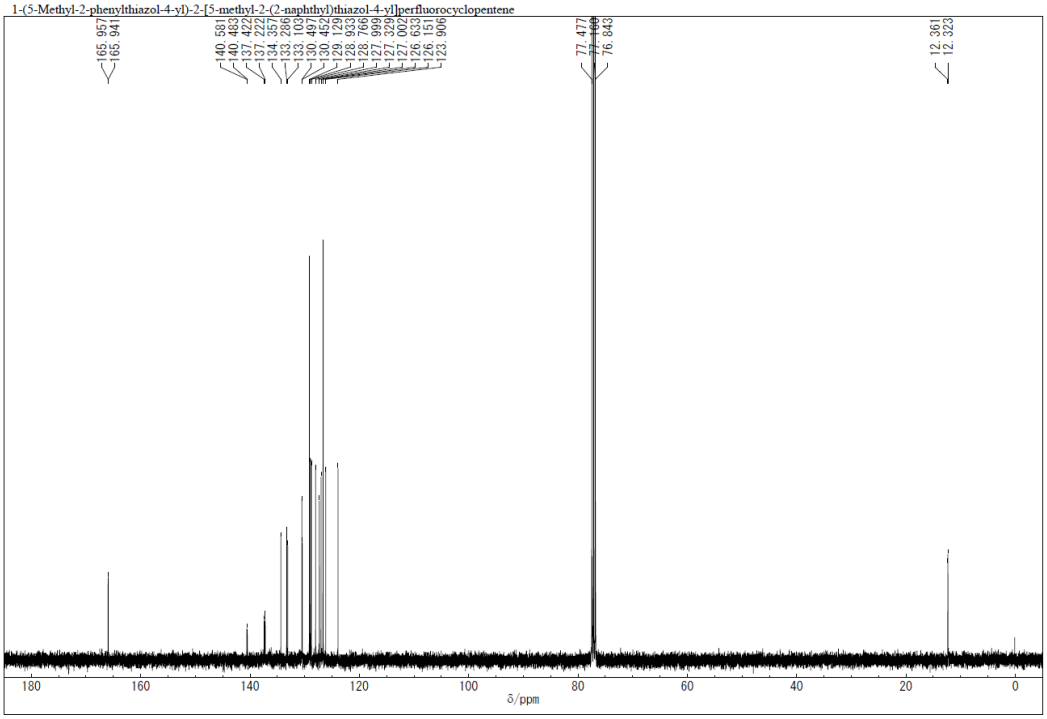

Figure S4. ^{13}C NMR ($CDCl_3$, 100 MHz) spectrum of 1-(5-methyl-2-phenylthiazol-4-yl)-2-[5-methyl-2-(2-naphthyl)thiazol-4-yl]perfluorocyclopentene (**1o**).

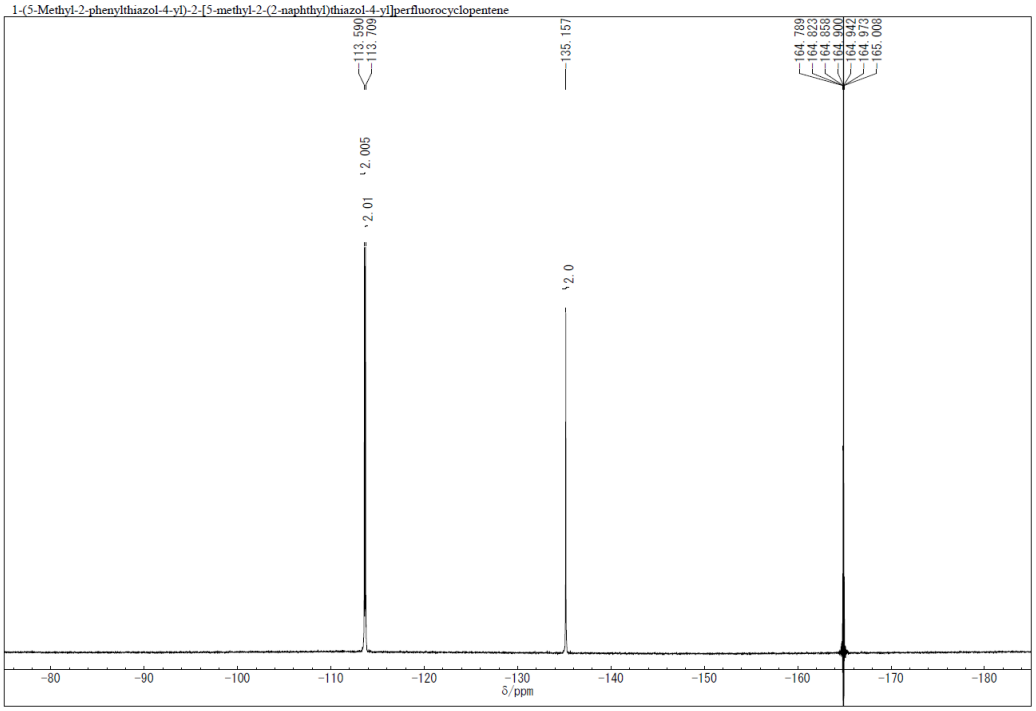

Figure S5. ^{19}F NMR ($CDCl_3$, 376 MHz) spectrum of 1-(5-methyl-2-phenylthiazol-4-yl)-2-[5-methyl-2-(2-naphthyl)thiazol-4-yl]perfluorocyclopentene (**1o**).

Fabrication of closed-ring isomer 1c

Into a 1000-mL Erlenmeyer flask, 15.6 mg of **1o** was added to 1000 mL of *n*-hexane and dissolved. Into a 100-mL screw tube bottle containing a stirrer, 70 mL of the solution was added, and the solution was irradiated with UV light (λ = 313 nm, 50 s) while stirring to obtain the photostationary state. The remaining solution was subjected to the same procedure, and then the solvent was removed. By recrystallization from *n*-hexane, 8.6 mg of the **1c** was obtained.

m.p. 237.0−237.9°C. ^{1}H NMR (400 MHz, $CDCl_3$, ppm: Figure S6) δ 8.42 (s, 1 H), 8.12 (dd, J = 8.6, 2.0 Hz, 1H), 8.02-7.96 (m, 3H), 7.91 (t, J = 8.4 Hz, 2H), 7.65-7.56 (m, 3H), 7.53-7.49 (m, 2H), 2.07 (s, 3H), 2.06 (s, 3H). ^{13}C NMR (100 MHz, $CDCl_3$, ppm: Figure S7) δ 179.9, 179.8, 159.5, 136.0, 133.8, 132.8, 132.6, 131.2, 130.1, 129.5, 129.4, 129.1, 129.0, 128.9, 128.1, 127.3, 124.9, 69.0, 25.4. 19F NMR (376 MHz, $CDCl_3$, ppm: Figure S8) δ -114.9 (dd, J = 260.0, 32.0 Hz, 2 F), -118.0 (dd, J = 260.0, 27.4 Hz 2F), -136.8 (s, 2F).

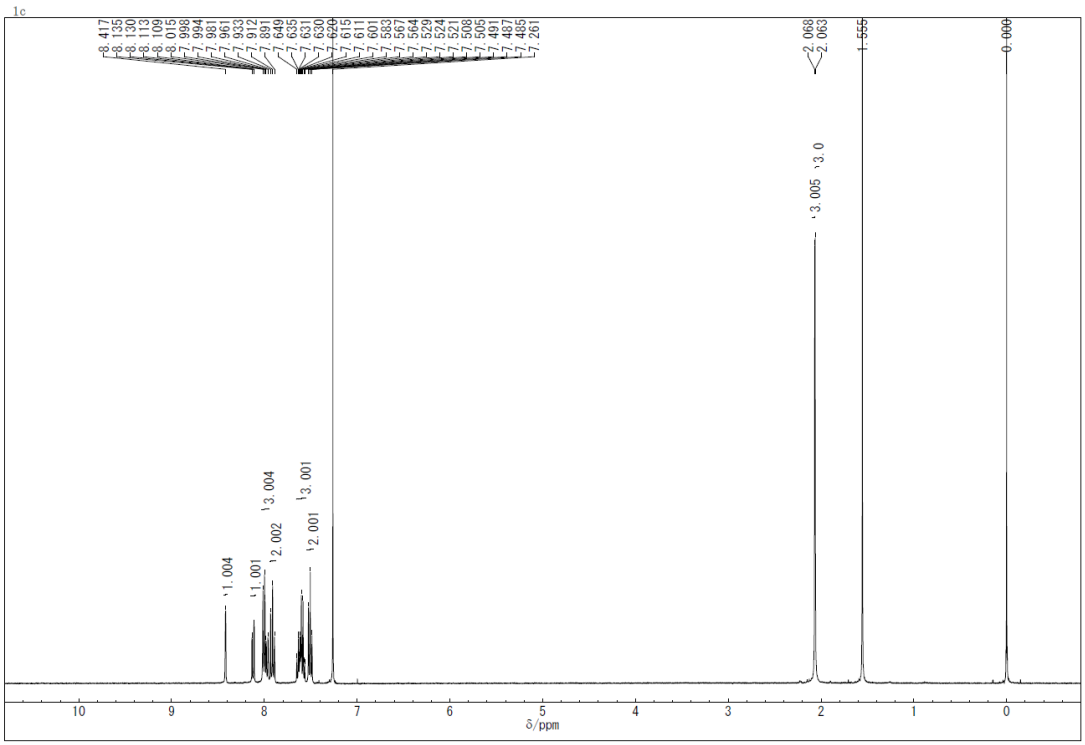

Figure S6. ^{1}H NMR ($CDCl_3$, 400 MHz) spectrum of **1c**.

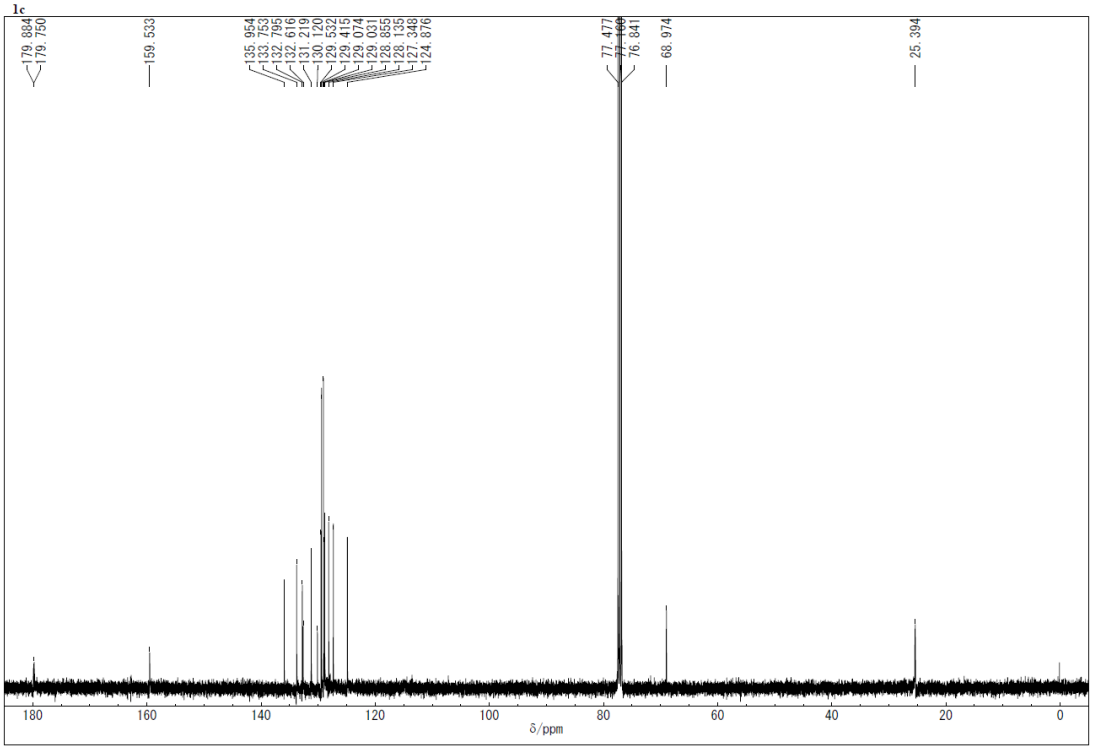

Figure S7. ^{13}C NMR ($CDCl_3$, 100 MHz) spectrum of **1c**.

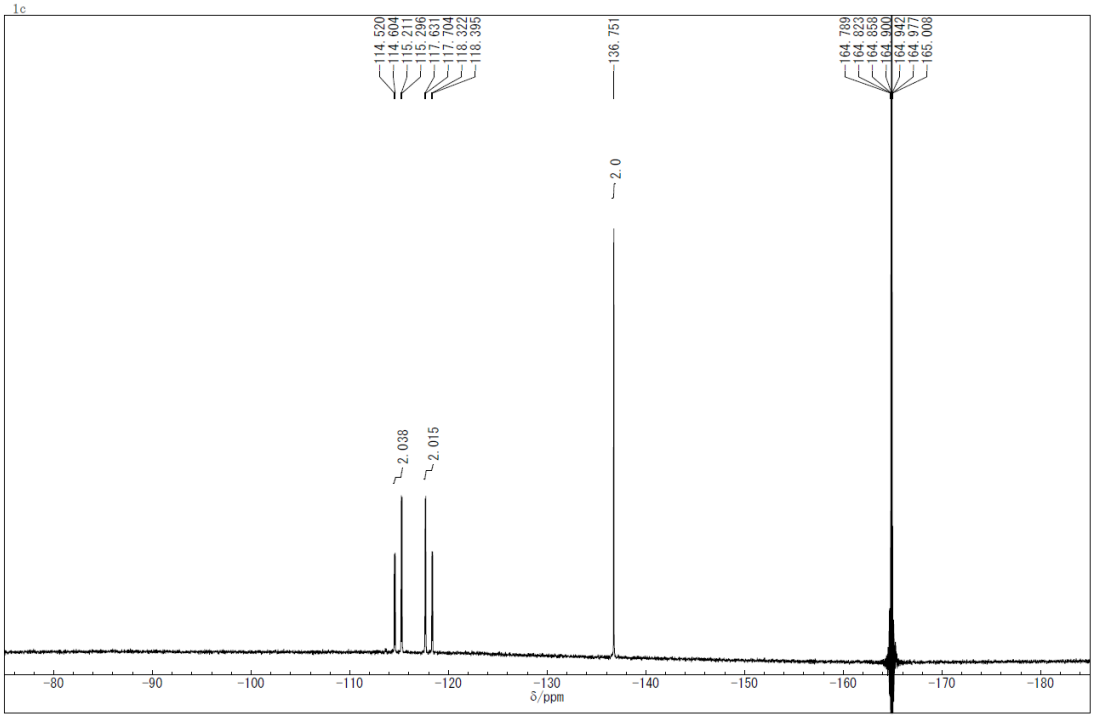

Figure S8. ^{19}F NMR ($CDCl_3$, 376 MHz) spectrum of **1c**.

6. Preparation of microcrystalline film

Into a 50-mL Erlenmeyer flask, 200 mg of **1o** was added to a mixed solvent of ethanol (32 mL) and water (8 mL). The mixture was heated to 60°C to dissolve the **1o**. Then, the solution was allowed to stand at room temperature for 24 h to allow the crystals to precipitate. The precipitated crystals were collected by suction filtration using Kiriyama filter paper (φ = 21 mm, No. 5A). The sample obtained after filtration was dried under reduced pressure for 24 h, forming **1o**-film.

7. Calculation of the influence ratio of intermolecular interactions in 1o crystals to each lattice axis

Crystal growth is affected by a variety of factors, such as intermolecular interactions, solvents, supersaturation ratios, and temperature. Among them, the crystals generally prefer to grow along the direction of strong intermolecular interactions. Here, we discuss the influence of T-shaped CH-π interactions and π-π stacking formed between naphthyl groups of different molecules on the growth of the crystal. The direction of formation of the interactions as viewed along each lattice axis obtained from X-ray crystal structure, is shown in Figures S14 and S15. The direction of interactions has three-dimensional coordinates. For simplicity, we calculated the angle (θ) at which the interaction was formed with respect to an axis from the two-dimensional coordinates as viewed from each lattice axis. From these calculated angles, the ratio of the influence to each lattice axis was calculated.

When viewed along *a*-axis a, the ratio of the influence of the interactions on the *c*-axis ($I^{\text{viewed along } a\text{-axis}}{}_{c\text{-axis}}$) is given by

$$I^{\text{viewd along } a-\text{axis}}{}_{c-\text{axis}} = \frac{\theta^{\text{viewd along } a-\text{axis}}{}_{\text{with respect to the } b-\text{axis}}}{\alpha}, \qquad (7)$$

where α is the angle formed by the *b*- and *c*-axes (Table 1). Since the influence ratio of the interaction on the *b*-axis ($I^{\text{viewed along } a\text{-axis}}{}_{b\text{-axis}}$) is the total minus the influence ratio of the interaction on the *c*-axis, it is given by

$$I^{\text{viewd along } a-\text{axis}}{}_{b-\text{axis}} = \frac{\theta^{\text{viewd along } a-\text{axis}}{}_{\text{with respect to the } c-\text{axis}}}{\alpha}$$
$$= 1 - I^{\text{viewd along } a-\text{axis}}{}_{c-\text{axis}}. \qquad (8)$$

When viewed along *b*-axis a, the ratio of the influence of the interactions on the *a*-axis ($I^{\text{viewed along } b\text{-axis}}{}_{a\text{-axis}}$) is given by

$$I^{\text{viewd along } b-\text{axis}}{}_{a-\text{axis}} = \frac{\theta^{\text{viewd along } b-\text{axis}}{}_{\text{with respect to the } c-\text{axis}}}{\beta}, \qquad (9)$$

where β is the angle formed by the *a*- and *c*-axes (Table 1). Since the influence ratio of the interaction on the *c*-axis ($I^{\text{viewed along } b\text{-axis}}{}_{c\text{-axis}}$) is the total minus the influence ratio of the interaction on the *a*-axis, it is given by

$$I^{\text{viewd along } b-\text{axis}}{}_{c-\text{axis}} = \frac{\theta^{\text{viewd along } b-\text{axis}}{}_{\text{with respect to the } a-\text{axis}}}{\beta} = 1 - I^{\text{viewd along } a-\text{axis}}{}_{a-\text{axis}}. \quad (10)$$

When viewed along *c*-axis a, the ratio of the influence of the interactions on the *b*-axis ($I^{\text{viewed along } c\text{-axis}}{}_{b\text{-axis}}$) is given by

$$I^{\text{viewd along } c-\text{axis}}{}_{b-\text{axis}} = \frac{\theta^{\text{viewd along } c-\text{axis}}{}_{\text{with respect to the } a-\text{axis}}}{\gamma}, \quad (11)$$

where γ is the angle formed by the *a*- and *b*-axes (Table 1). Since the influence ratio of the interaction on the *a*-axis ($I^{\text{viewed along } c\text{-axis}}{}_{a\text{-axis}}$) is the total minus the influence ratio of the interaction on the *b*-axis, it is given by

$$I^{\text{viewd along } c-\text{axis}}{}_{a-\text{axis}} = \frac{\theta^{\text{viewd along } c-\text{axis}}{}_{\text{with respect to the } b-\text{axis}}}{\gamma} = 1 - I^{\text{viewd along } c-\text{axis}}{}_{b-\text{axis}}. \quad (12)$$

The ratio of the total interaction in three-dimensional coordinates is determined using the ratio of interactions calculated from each axis when viewed along the *a*-, *b*-, and *c*-axes, and it is given by

$$I^{\text{total}}{}_{a-\text{axis}} = \frac{I^{\text{viewd along } b-\text{axis}}{}_{a-\text{axis}} + I^{\text{viewd along } c-\text{axis}}{}_{a-\text{axis}}}{3}, \quad (13)$$

$$I^{\text{total}}{}_{b-\text{axis}} = \frac{I^{\text{viewd along } a-\text{axis}}{}_{b-\text{axis}} + I^{\text{viewd along } c-\text{axis}}{}_{b-\text{axis}}}{3}, \quad (14)$$

$$I^{\text{total}}{}_{c-\text{axis}} = \frac{I^{\text{viewd along } a-\text{axis}}{}_{c-\text{axis}} + I^{\text{viewd along } b-\text{axis}}{}_{c-\text{axis}}}{3}. \quad (15)$$

In the system of **1o** crystal, the interactions between the naphthyl groups of different molecules are T-shaped CH-π interaction ($I^{\text{total (CH-}\pi\text{)}}$) and non-overlapping π-π stacking ($I^{\text{total (}\pi\text{-}\pi\text{)}}$). The ratio of T-shaped CH-π interaction to non-overlapping π-π stacking was 3:4 when viewed in a supercell shown as 2 × 2 × 2 unit cells from the X-ray crystal structure (Main text, Figure 4). Taking this into account, the average of the ratio of influence of these interactions ($I^{\text{Avg.}}$) was determined by the following equations:

$$I^{\text{Avg.}}{}_{a-\text{axis}} = \frac{I^{\text{total (CH}-\pi\text{)}}{}_{a-\text{axis}} \times 3 + I^{\text{total (}\pi-\pi\text{)}}{}_{a-\text{axis}} \times 4}{7}, \quad (16)$$

$$I^{\text{Avg.}}{}_{b-\text{axis}} = \frac{I^{\text{total (CH}-\pi\text{)}}{}_{b-\text{axis}} \times 3 + I^{\text{total (}\pi-\pi\text{)}}{}_{b-\text{axis}} \times 4}{7}, \quad (17)$$

$$I^{\text{Avg.}}{}_{c-\text{axis}} = \frac{I^{\text{total (CH}-\pi)}{}_{c-\text{axis}} \times 3 + I^{\text{total }(\pi-\pi)}{}_{c-\text{axis}} \times 4}{7}. \quad (18)$$

These calculated values are summarized in Table S7.

Figures and Tables

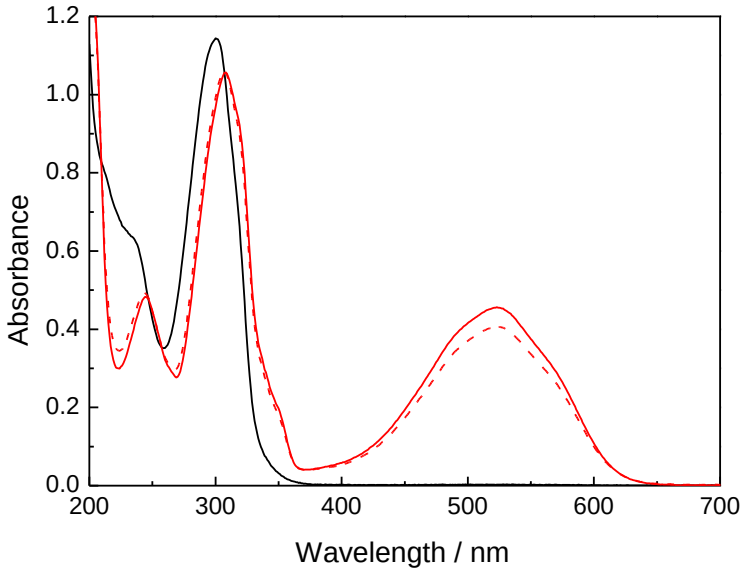

Figure S9. Absorption spectra of **2** in *n*-hexane solution. **2o**: solid black line, **2c**: solid red line, photostationary state (**2o**:**2c** = 11:89) upon 313 nm light irradiation: broken red line. These data were adapted from Y. Nakagawa et al. Photoinduced cytotoxicity of photochromic symmetric diarylethene derivatives: the relation of structure and cytotoxicity. *Org. Biomol. Chem.* 2022, **20**, 3211−3217.[S8]

Figure S10. (a) Photograph of a **1o-film** separated from the filter paper. (b, c) Photographs of the front and back sides of **1o-film** before (b) and after UV (λ = 365 nm) light irradiation (c). (d) Specular reflectance spectra of back side of **1o-film** before and after UV light irradiation from the front side.

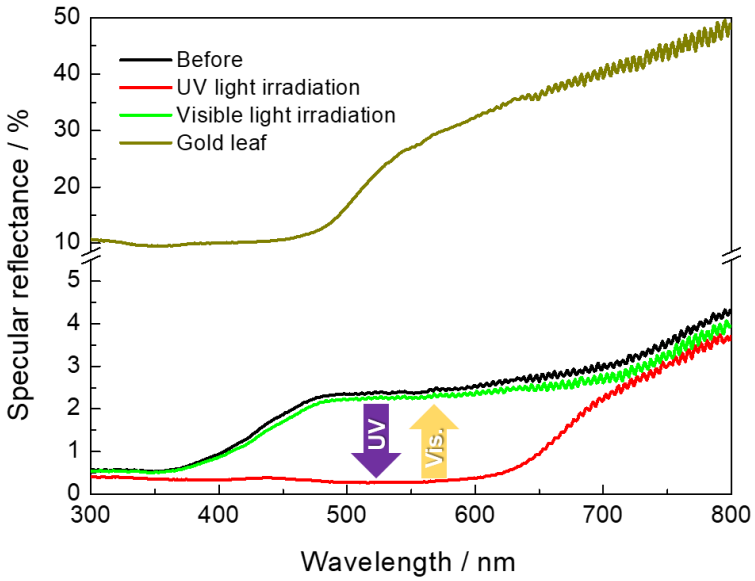

Figure S11. Specular reflectance and spectral changes of **1o-film** by UV-visible light irradiation and specular reflectance spectrum of gold leaf. Similar to gold leaf, the **1o-film** is characterized by absorption in the violet (380–450 nm) and blue (450–495 nm) regions.

Table S1. CIELAB color coordinates for **1o-film**.

	L*	a*	b*
1o-film	92.6967	-8.9569	26.5941
1o-film (UV)	37.5267	19.4433	-2.1689
1o-film (UV-Vis.)	92.8351	-9.0860	26.7721

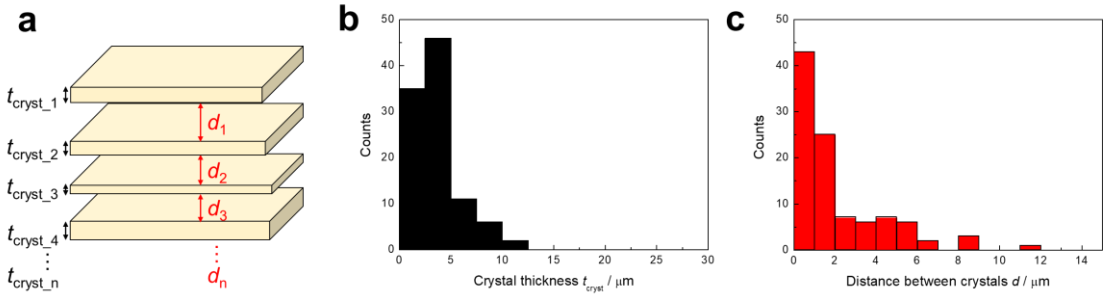

Figure S12. (a) Schematic illustration for calculating thickness of crystals and distance between crystals of **1o-film**. (b) Distribution of thickness of the crystals in **1o-film**. Here, crystal thickness (t_{cryst}) was delimited (Table S2), and the number of crystals in that range was counted. Crystal thickness was calculated by extracting 100 samples from cross-sectional SEM images of **1o-film**. (c) Distribution of distance between crystals of **1o-film**. Here, distance between crystals (d) was delimited (Table S3), and the amount of distance between crystals in that range was measured. The distance between crystals was calculated by extracting 100 samples from cross-sectional SEM images of **1o-film**.

Table S2. Delimitation of crystal thickness (t_{cryst}) in distribution and number of counts in **1o-film**.

Interval / μm	Counts
$0 < t_{cryst} \leq 2.5$	35
$2.5 < t_{cryst} \leq 5$	46
$5 < t_{cryst} \leq 7.5$	11
$7.5 < t_{cryst} \leq 10$	6
$10 < t_{cryst} \leq 12.5$	2
$12.5 < t_{cryst} \leq 15$	0
$15 < t_{cryst} \leq 17.5$	0
$17.5 < t_{cryst} \leq 20$	0
$20 < t_{cryst} \leq 22.5$	0
$22.5 < t_{cryst} \leq 25$	0
$25 < t_{cryst} \leq 27.5$	0
$27.5 < t_{cryst} \leq 30$	0

Table S3. Delimitation of distance between crystals (*d*) in distribution and number of counts in **1o-film**.

Interval / μm	Counts
0 < *d* ≤ 1	43
1 < *d* ≤ 2	25
2 < *d* ≤ 3	7
3 < *d* ≤ 4	6
4 < *d* ≤ 5	7
5 < *d* ≤ 6	6
6 < *d* ≤ 7	2
7 < *d* ≤ 8	0
8 < *d* ≤ 9	3
9 < *d* ≤ 10	0
10 < *d* ≤ 11	0
11 < *d* ≤ 12	1
12 < *d* ≤ 13	0
13 < *d* ≤ 14	0
14 < *d* ≤ 15	0

Table S4. Thickness of crystal and distance between crystals in **1o-film**.

Compound	Thickness t_{cryst}: Ave. ± S.D. / μm	Distance between crystals *d*: Ave. ± S.D. / μm
1	3.7 ± 2.2	2.2 ± 2.1

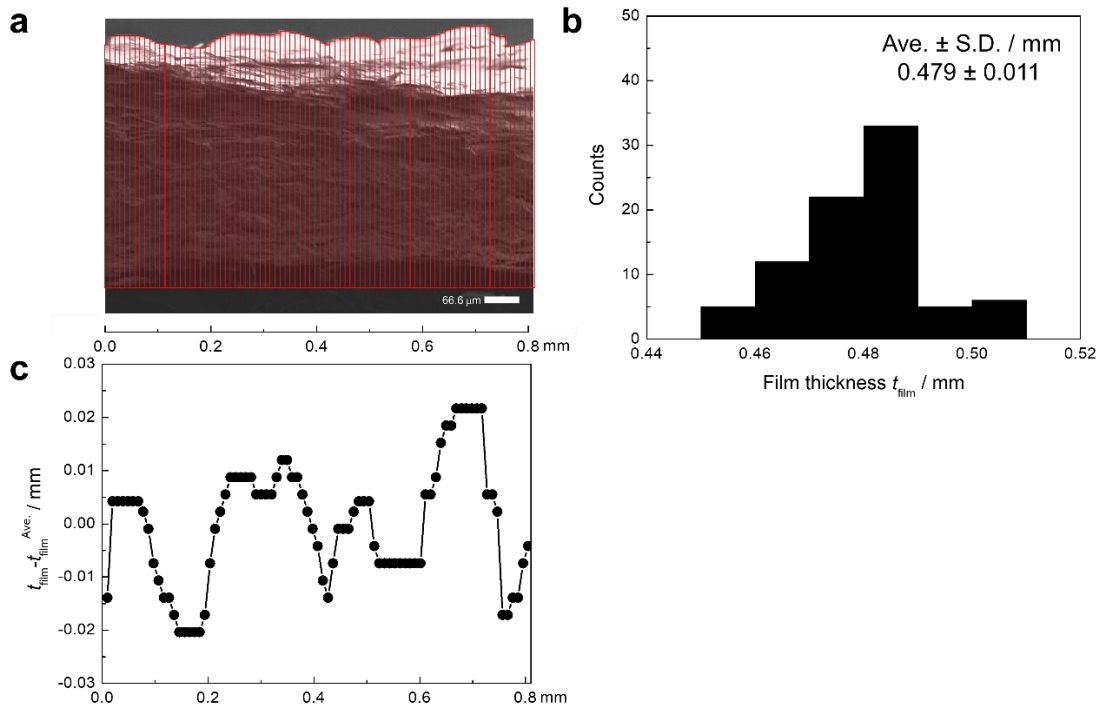

Figure S13. (a) Cross-sectional SEM image of **1o-film**. (b) Distribution of the film thickness of **1o-film**. Here, the film thickness (t_{film}) was delimited as shown in Table S5, and the number of film thicknesses in that range was counted. Film thickness was calculated by extracting 83 samples from cross-sectional SEM images of **1o-film** as shown in Figure S13a. (c)

Table S5. Delimitation of film thickness (t_{film}) in distribution and number of counts in **1o-film**.

Interval / μm	Counts
$0.45 < t_{film} \leq 0.46$	5
$0.46 < t_{film} \leq 0.47$	12
$0.47 < t_{film} \leq 0.48$	22
$0.48 < t_{film} \leq 0.49$	33
$0.49 < t_{film} \leq 0.50$	5
$0.50 < t_{film} \leq 0.51$	6

Table S6. Crystal data of **2o**.[S7]

	2o
Formula	$C_{25}H_{16}F_6N_2S_2$
Formula weight	522.53
T/K	93(2)
Crystal system	monoclinic
Space group	$P2_1/c$
a / Å	7.2354(2)
b / Å	25.7171(11)
c / Å	12.6083(5)
α / °	90
β / °	102.3200(13)
γ / °	90
V / Å^3	2292.04(15)
Z	4
R_1 (I > 2σ(I))	0.0322
wR_2 (I > 2σ(I))	0.0713
R_1 (all data)	0.0408
wR_2 (all data)	0.0760
CCDC No.	1870382

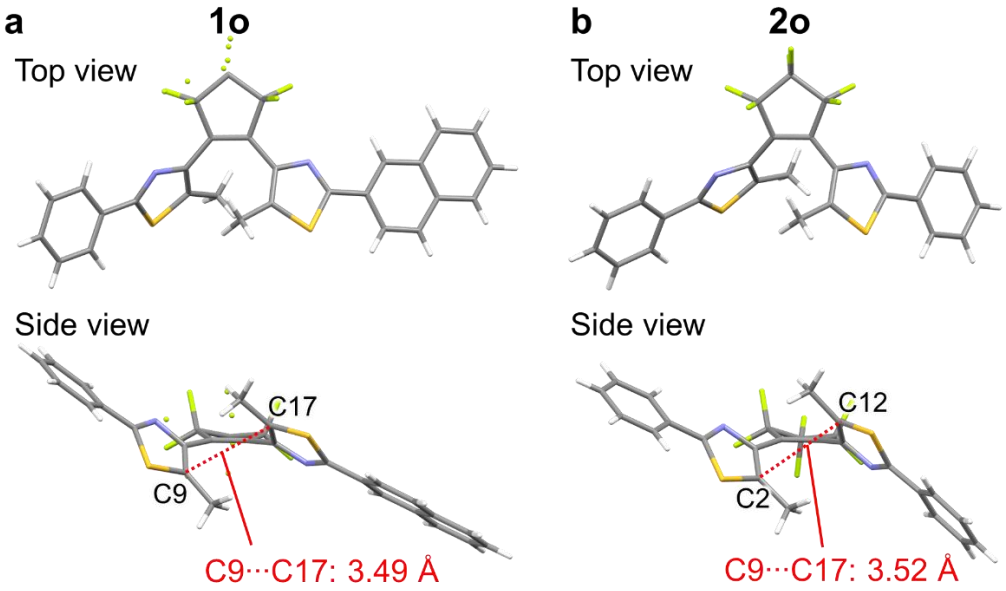

Figure S14. Molecular structures in single crystal of (a) **1o** and (b) **2o**.

Table S7. Geometric parameters of crystal structures of **1o** and **2o**.

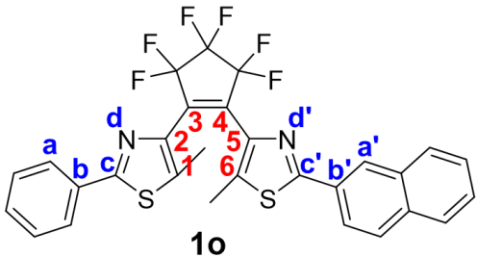

1o

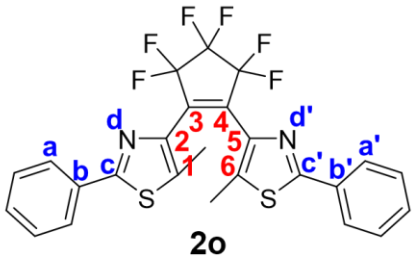

2o

φ_1 = ∢(C_1, C_2, C_3, C_4), φ_2 = ∢(C_3, C_4, C_5, C_6)
θ_1 = ∢(C_a, C_b, C_c, C_d), θ_2 = ∢($C_{a'}$, $C_{b'}$, $C_{c'}$, $C_{d'}$)

	1o	**2o**
$r_{C1\text{-}C6}$ [Å]	3.49	3.52
φ_1 [degree]	-44.3	-43.5
φ_2 [degree]	-39.3	-46.0
θ_1 [degree]	24.0	16.3
θ_2 [degree]	12.9	8.3

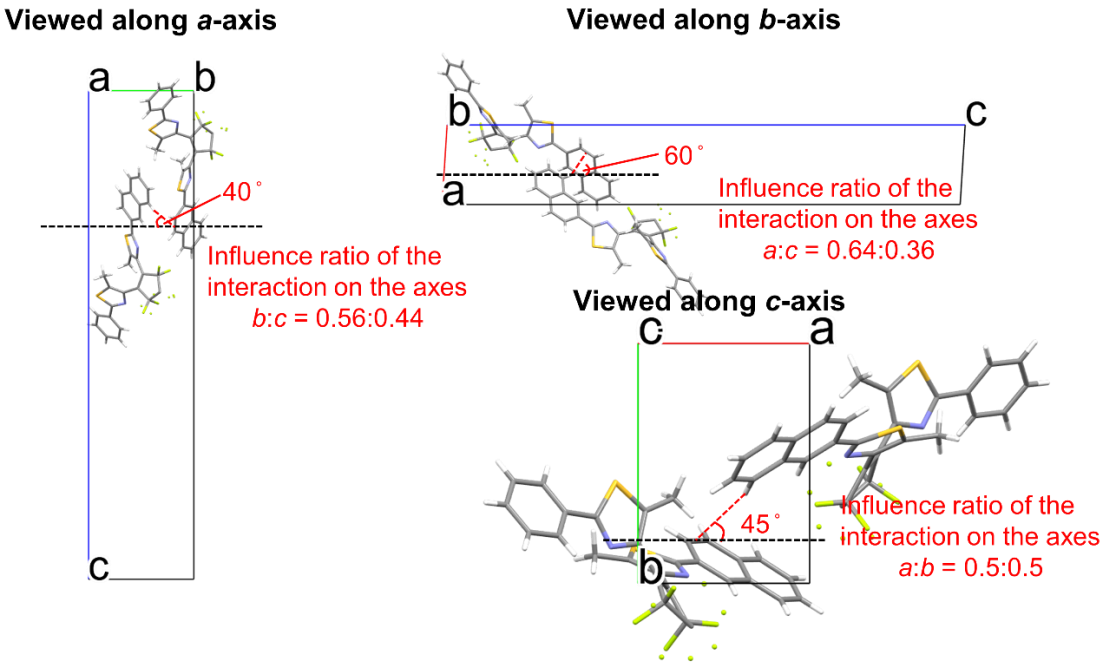

Figure S15. Ratio of influence on each lattice axis due to T-shaped CH-π interaction between naphthyl groups of different molecules in a **1o** crystal.

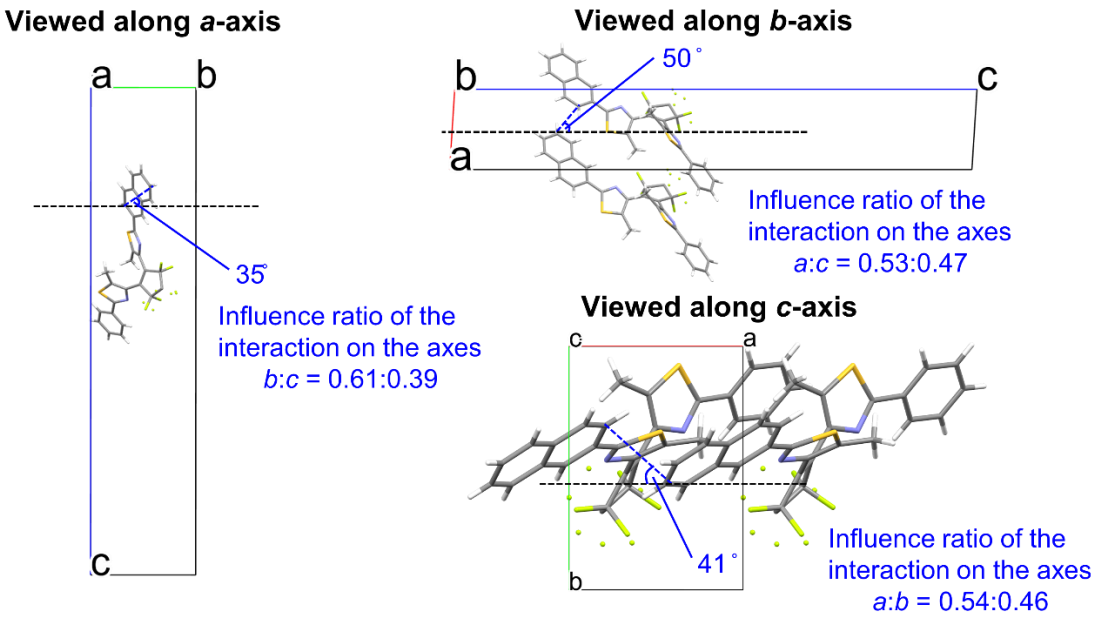

Figure S16. Ratio of influence on each lattice axis due to π-π interaction between naphthyl groups of different molecules in a **1o** crystal.

Table S8. Ratio of influence of each axis, based on T-shaped CH-π interaction, π-π stacking, and average of these interactions.

	Influence ratio of interaction on axes		
	$I^{total\ (CH-\pi)}$	$I^{total\ (\pi-\pi)}$	$I^{Avg.}$
a-axis	0.38	0.36	0.37
b-axis	0.35	0.36	0.36
c-axis	0.27	0.28	0.27

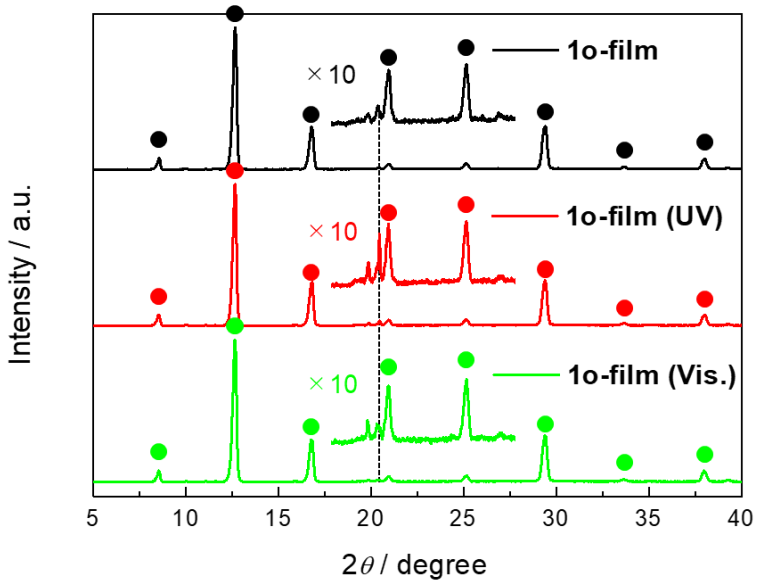

Figure S17. XRD patterns of **1o-film** before and after UV (λ = 365 nm, 30 s)-visible light (λ > 480 nm, 5 min) irradiation. The circles indicate the peak of lamellar spacing peak. The continuous periodic diffraction from 2nd to 9th order was maintained even after UV-visible light irradiation. The dotted line indicates a new peak that appeared upon UV light irradiation. This peak disappeared upon subsequent visible light irradiation.

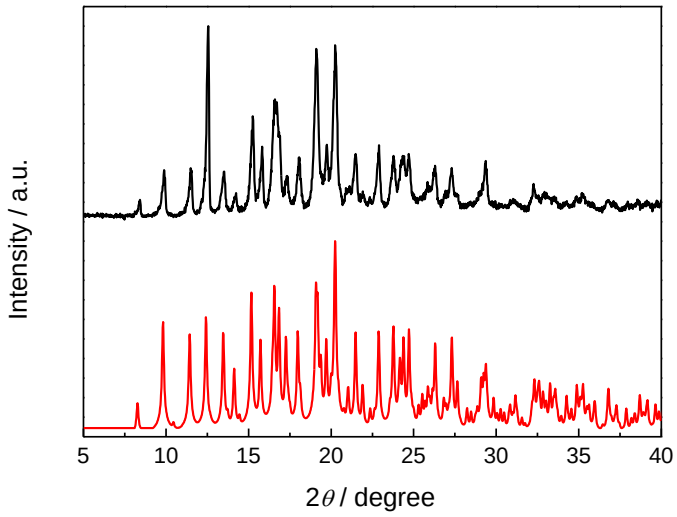

Figure S18. XRD pattern of powder of **1o** (black) and pattern calculated from single-crystal X-ray crystallographic data of **1o** (red). The powder of **1o** was prepared by grinding **1o-film**.

References

[S1] H. E. Gottlieb, V. Kotlyar, A. Nudelman, *J. Org. Chem.* 1997, **62**, 7512–7515.

[S2] C. A. Schneider, W. S. Rasband, K. W. Eliceiri, *Nat. Methods* 2012, **9**, 671−675.

[S3] International Color Consortium. Specification ICC.1:2022 (Profile version 4.4.0.0)

[S4] J. Schanda in *Colorimetry: understanding the CIE system* (Ed.: J. Schanda), New Jersey, John Wiley &Sons, 2007, p. 25–76.

[S5] W. S. Stiles, J. M. Birch, *Opt Acta* 1959, **6**, 1–26.

[S6] H. Nishi, T. Namari, S. Kobatake, *J. Mater. Chem.* 2011, **21**, 17249–17258.

[S7] Y. Nakagawa, M. Morimoto, N. Yasuda, K. Hyodo, S. Yokojima, S. Nakamura, K. Uchida, *Chem. – Eur. J.* 2019, **25**, 7874−7880.

[S8] Y. Nakagawa, T. Hishida, E. Hatano, K. Sumaru, K. Morishita, M. Morimoto, S. Yokojima, S. Nakamura, K. Uchida, *Org. Biomol. Chem.* 2022, **20**, 3211−3217.